THE JOURNAL OF BIOLOGICAL CHEMISTRY VOL. 291, NO. 31, pp. 16059–16067, July 29, 2016

Phosphorylation Interferes with Maturation of Amyloid-β Fibrillar Structure in the N Terminus*

Received for publication, March 24, 2016, and in revised form, May 30, 2016 Published, JBC Papers in Press, June 1, 2016, DOI 10.1074/jbc.M116.728956

Nasrollah Rezaei-Ghaleh[‡§1], Sathish Kumar[¶], Jochen Walter[¶], and Markus Zweckstetter[‡§‖2]

From the [‡]German Center for Neurodegenerative Diseases (DZNE), Von-Siebold-Strasse 3a, 37075 Göttingen, Germany, [§]Department for NMR-based Structural Biology, Max Planck Institute for Biophysical Chemistry, Am Fassberg 11, 37077 Göttingen, Germany, [¶]Department of Neurology, University of Bonn, 53127 Bonn, Germany, and [‖]Department of Neurology, University Medical Center, University of Göttingen, Göttingen, Waldweg 33, 37073 Göttingen, Germany

Neurodegeneration is characterized by the ubiquitous presence of modifications in protein deposits. Despite their potential significance in the initiation and progression of neurodegenerative diseases, the effects of posttranslational modifications on the molecular properties of protein aggregates are largely unknown. Here, we study the Alzheimer disease-related amyloid-β (Aβ) peptide and investigate how phosphorylation at serine 8 affects the structure of Aβ aggregates. Serine 8 is shown to be located in a region of high conformational flexibility in monomeric Aβ, which upon phosphorylation undergoes changes in local conformational dynamics. Using hydrogen-deuterium exchange NMR and fluorescence quenching techniques, we demonstrate that Aβ phosphorylation at serine 8 causes structural changes in the N-terminal region of Aβ aggregates in favor of less compact conformations. Structural changes induced by serine 8 phosphorylation can provide a mechanistic link between phosphorylation and other biological events that involve the N-terminal region of Aβ aggregates. Our data therefore support an important role of posttranslational modifications in the structural polymorphism of amyloid aggregates and their modulatory effect on neurodegeneration.

Aggregation of the amyloid-β (Aβ)[3] peptide into oligomers, protofibrils, and amyloid fibrils is the pathological hallmark of Alzheimer disease (AD) (1). Neurotoxic protein aggregation is often characterized by high levels of posttranslational modifications (2, 3). A particularly abundant modification in amyloid deposits is phosphorylation (4). For example, the Tau protein found in intracellular neurofibrillary tangles of AD brains is hyperphosphorylated, and in Lewy bodies in Parkinson disease brains, a large fraction of α-synuclein is phosphorylated at serine 129 (4). In the case of Aβ, it has been shown that phosphorylation at Ser^{26} is particularly abundant in intraneuronal deposits at very early stages of AD (5), whereas phosphorylation at Ser^8 is detected in the later stages of the disease (6).

Several aspects of protein activity are influenced by phosphorylation of neurodegeneration-related proteins (4). It has been shown that phosphorylation of the Parkinson disease-related α-synuclein alters its interactions with other proteins (7) and membrane lipids (8) and plays a role in regulating its subcellular localization (9) and degradation (10–12). In the case of Aβ, phosphorylation at Ser^8 attenuates its proteolytic degradation by certain proteases (13). It has also been suggested that the Ser^8 phosphorylation level defines the biochemical stage of Aβ aggregate maturation, which is associated with the conversion from preclinical to symptomatic AD (6, 14). Despite its mechanistic importance, little is known on the effect of phosphorylation on the molecular properties of protein aggregates, especially their structure.

Progress over the past decade has provided substantial insight into the structure of Aβ fibrils (15, 16). In most models, Aβ molecules adopt a U-shaped β-strand-turn-β-strand fold. Despite the fact that the N-terminal region of Aβ is mainly unstructured in these fibrillar models, several lines of evidence point to an important role of this region in pathogenic aggregation. In particular, it has been shown that toxic Aβ assembly is enhanced by mutations in this region (A2V, H6R, or D7N) (17, 18) as well as N-terminal truncation with or without pyroglutamate formation (19, 20). Furthermore, antibodies against the N-terminal region inhibit Aβ amyloid formation (21), and the conformational propensity of the N-terminal region controls the partitioning between Aβ oligomers and protofibrils (22). In addition, phosphorylation at Ser^8 promotes toxic Aβ aggregation both *in vitro* and *in vivo* (23) and increases the stability of Aβ aggregates against pressure- and SDS-induced dissociation into monomers (24).

Because of their putative role in the initiation and spreading of neurodegenerative diseases and their potential as therapeutic targets, there is growing interest in elucidating the effects of posttranslational modifications on the molecular properties of protein aggregates (4). In the present study, we used hydrogen-deuterium exchange coupled with solution-state NMR techniques and demonstrated that phosphorylation of Ser^8 favors more exposed conformations in the N-terminal region of Aβ in insoluble aggregates. Our data support an important role of posttranslational modifications in the structural polymorphism of amyloid protein deposits and suggest a modulatory role in the course and severity of neurodegenerative diseases.

* The authors declare that they have no conflicts of interest with the contents of this article.

[1] To whom correspondence may be addressed: German Center for Neurodegenerative Diseases (DZNE), Von-Siebold-Str. 3a, 37075 Göttingen, Germany. Fax: 49-551-201-2202; E-mail: nare@nmr.mpibpc.mpg.de.

[2] To whom correspondence may be addressed: German Center for Neurodegenerative Diseases (DZNE), Von-Siebold-Str. 3a, 37075 Göttingen, Germany. Fax: 49-551-201-2202; E-mail: markus.zweckstetter@dzne.de.

[3] The abbreviations used are: Aβ, amyloid-β; AD, Alzheimer disease; npAβ, non-phosphorylated Aβ1-40; pS8Aβ, Ser^8-phosphorylated Aβ1-40; TOCSY, total correlation spectroscopy; CLEANEX-PM, phase-modulated CLEAN chemical exchange; K_{SV}, Stern-Volmer constant.

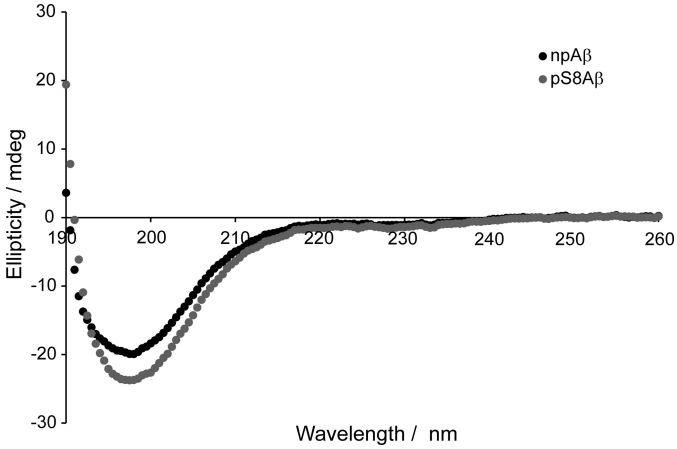

FIGURE 1. **Both wild-type and Ser[8]-phosphorylated Aβ are largely disordered in the monomeric state.** Far-UV CD spectra of freshly dissolved ("monomeric") states of both npAβ and pS8Aβ show spectral features that are characteristic for random coil conformation. *mdeg*, millidegrees.

Results

Monomeric Aβ Remains Disordered after Ser[8] Phosphorylation—First, we investigated the structural features of non-aggregated Aβ by CD and NMR. The far-UV CD spectra of both non-phosphorylated Aβ1–40 (npAβ) and Ser[8]-phosphorylated Aβ1–40 (pS8Aβ) were indicative of largely disordered conformations as manifested in prominent negative minima at ~199 nm and weak shoulders at ~218 nm (Fig. 1). The one-dimensional proton NMR spectra of the two peptides showed poor resonance dispersion in the amide and methyl regions, further supporting their lack of ordered structure (Fig. 2, *A* and *B*). Minor differences between the two spectra were observed in the amide and aromatic regions, including the expected downfield signal that originated from the amide proton of phosphoserine (at ~9.25 ppm) and two other peaks from the backbone amide proton of Tyr[10] and the side chain ϵ1 proton of His[6], both in the vicinity of the phosphorylated residue (Fig. 2*A*). In pulsed field gradient NMR experiments, the two peptides showed identical decay curves of NMR signal intensity, indicating that they had the same apparent diffusion coefficient of 8.27×10^{-7} $cm^2 \cdot s^{-1}$ at 5 °C and thus the same assembly state (Fig. 2*C*). A calculated hydrodynamic radius of ~1.6 nm demonstrated that the NMR-visible states of the two peptides were mainly monomeric.

Serine 8 Undergoes Extensive Conformational Dynamics in Monomeric Aβ—NMR chemical shifts are sensitive probes of local conformational dynamics in polypeptide chains. The random coil index (25) calculated from backbone chemical shifts (HN, HA, N, CA, and CO) of npAβ reveals that serine 8 is located in a region of high conformational flexibility in the N-terminal region of Aβ that extends down to residue Glu[11] (Fig. 3). Interestingly, Ser[26], the second potential site of Aβ phosphorylation, occurs in a region of high mobility too, although the mobility level of these two regions is quantitatively different. It has been shown that phosphorylation of Ser[26] results in a significant loss of conformational plasticity in Aβ that is otherwise essential for the progression of Aβ aggregation toward fibrils (26). It is therefore important to see how Ser[8] phosphorylation may influence the local conformational dynamics in Aβ.

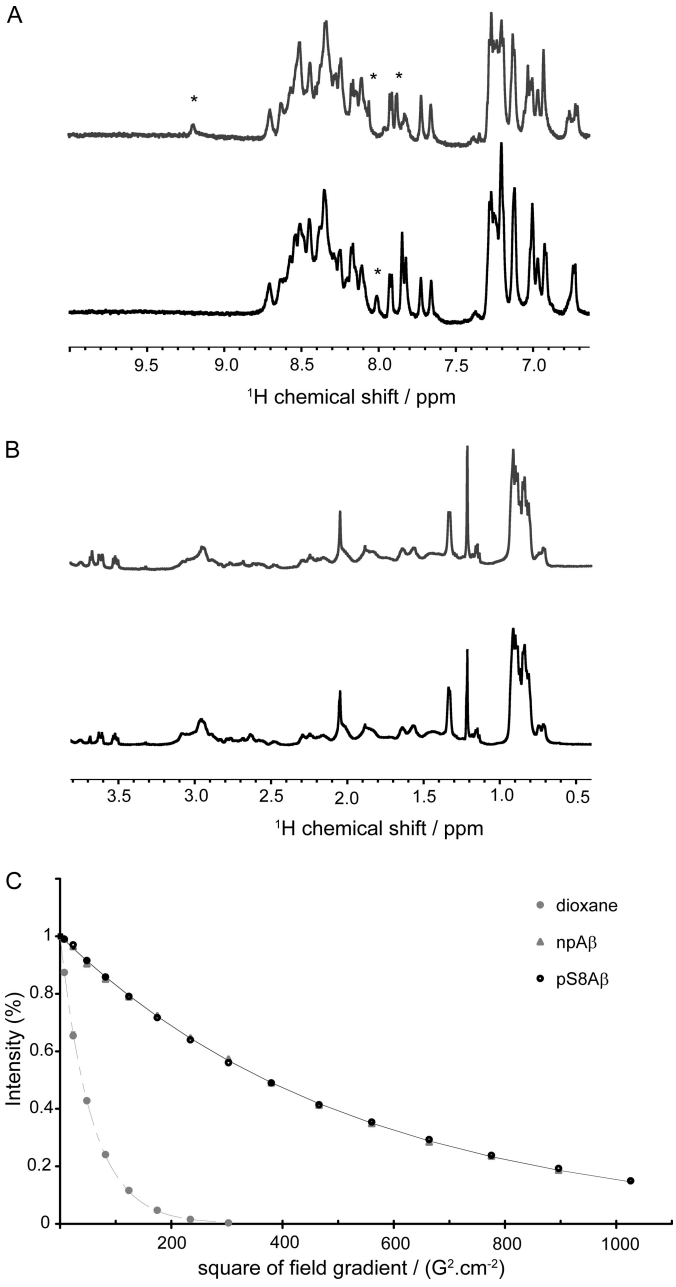

FIGURE 2. **Aβ peptide is in an unstructured monomeric state independent of the phosphorylation state at Ser[8].** *A* and *B*, one-dimensional ^{1}H NMR spectra of npAβ (*black*) and pS8Aβ (*gray*) in the amide/aromatic (*A*) and aliphatic/methyl (*B*) regions, respectively. The low chemical shift dispersion of amide and methyl proton resonances is in agreement with the unstructured nature of the two peptides. Marked (*) peaks originate from the amide proton of phosphorylated Ser[8], the amide proton of Tyr[10], and the ϵ1H of His[6]. *C*, NMR signal decay observed for npAβ (*black*) and pS8Aβ (*gray*) at 5 °C in pulsed field gradient NMR experiments. To estimate the hydrodynamic radii, the signal decay of dioxane was also recorded. The data show that npAβ and pS8Aβ have identical diffusion coefficients in agreement with a similar assembly state.

Phosphorylation at Ser[8] Alters Local Conformational Dynamics of Aβ—The HN and HA chemical shifts obtained by two-dimensional homonuclear experiments showed that the backbone conformation of npAβ and pS8Aβ differs mainly around the phosphorylation site. The largest chemical shift

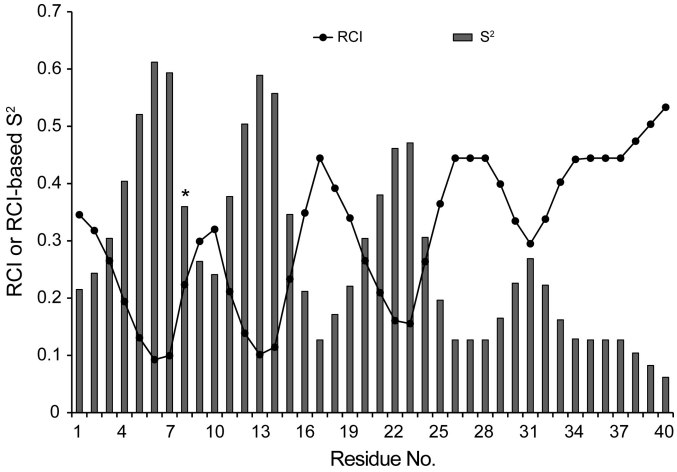

FIGURE 3. **Serine 8 is located in a region of high conformational flexibility in the N-terminal region of Aβ.** The random coil index (*RCI*) and random coil index-based squared order parameter (S^2), derived from the backbone chemical shifts of Aβ, are shown. Serine 8, marked by an *asterisk*, along with residues Gly^9–Glu^{11}, exhibit higher mobility than the flanking residues Arg^5–Asp^7 and Val^{12}–His^{14}.

deviations were observed at Ser^8 and Asp^7 followed by residues 4–16 (Fig. 4*A*). The amide proton of His^6 was not detectable in npAβ, probably due to severe exchange broadening, but with pS8Aβ, a strong His^6 HA-HN correlation peak was observed. The signs of HA shift changes were opposite for residues preceding and following Ser^8: Phe^4, Asp^7, and Ser^8 rose in HA shift, whereas residues 9–12 fell (Fig. 4*A*, *inset*). This suggests a differential influence of phosphorylation on these residues: the conformation of the N-terminal residues gets more extended, whereas succeeding residues tend to become less extended. The latter is in line with enhanced HN(*i*)-HN(*i* + 1) NOE peaks of residues Gly^9–Glu^{11} in pS8Aβ (Fig. 4, *B* and *C*). The side chain resonances of Asp^7 and Tyr^{10} provided further support for the differential impact of Ser^8 phosphorylation on the structural dynamics downstream and upstream of the phosphorylation site. The two HB resonances of Asp^7, unresolved in npAβ, became well separated following phosphorylation, whereas the two well resolved HB resonances of Tyr^{10} in npAβ lost their dispersion upon phosphorylation (Fig. 5). Notably, a significant increase in the intensity of sequential NOE peaks between the amide protons of residues Asp^{23}–Gly^{25} and Gly^{29}-Ala^{30} was also observed, suggesting that a long range conformational change may occur after Ser^8 phosphorylation. Together, our data show that monomeric Aβ preserves its disordered structure in the Ser^8-phosphorylated state with structural changes mainly induced around the site of phosphorylation.

Phosphorylation at Ser^8 Decreases Compaction of Aβ Aggregates in the N-terminal Region—Next, the effect of Ser^8 phosphorylation on the structure of aggregated Aβ was investigated. First, a control experiment confirmed that pS8Aβ possessed a higher rate and amount of thioflavin T-reactive aggregation than npAβ, in line with previous reports (data not shown) (23). Then we used hydrogen-deuterium exchange coupled to solution-state NMR to provide high resolution information on the backbone structure of Aβ aggregates dependent on Ser^8 phosphorylation. After 7 days of aggregation (37 °C with gentle stirring), which led to formation of amyloid fibrillar aggregates, the

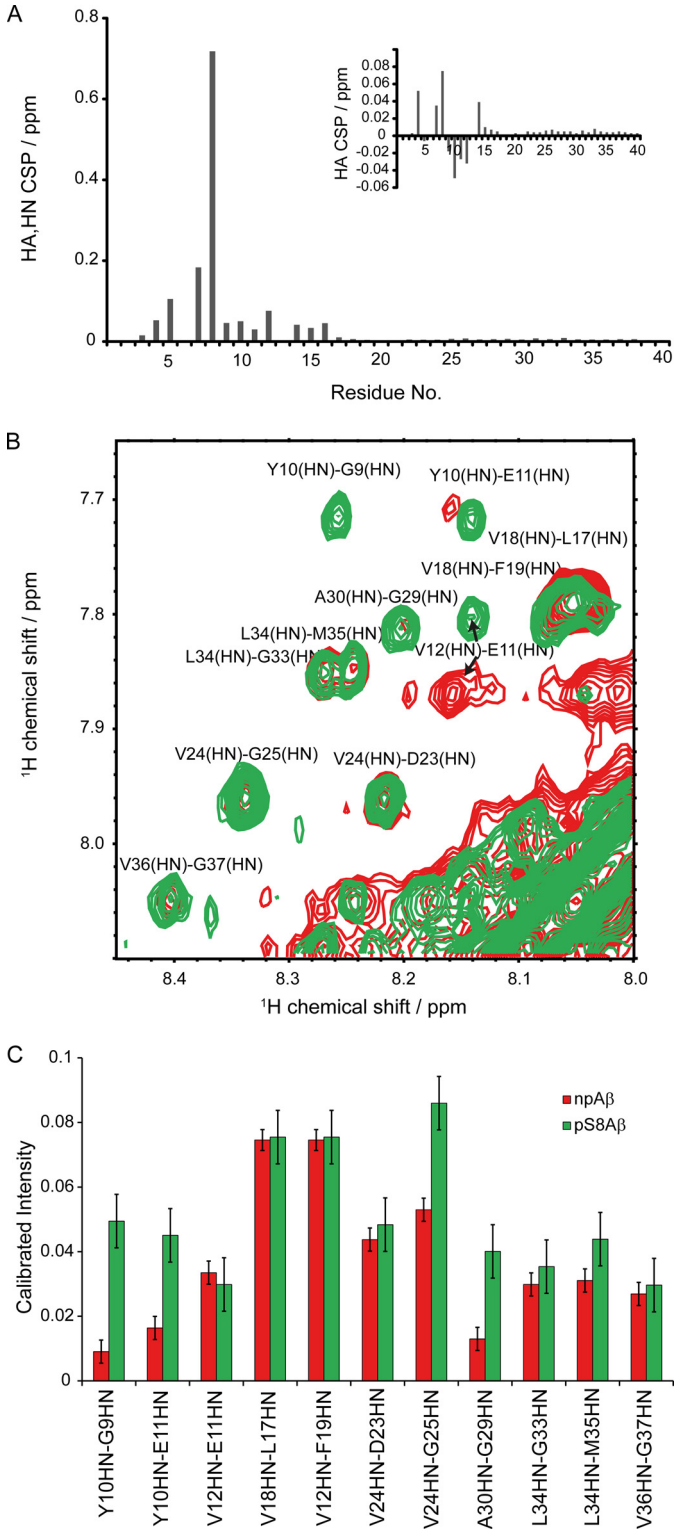

FIGURE 4. **Effect of Ser^8 phosphorylation on the structure of monomeric Aβ.** *A*, combined HA and HN chemical shift perturbation (*CSP*) indicates conformational changes around the phosphorylation site. In the *inset*, the HA chemical shift perturbations are shown. *B*, superposition of two-dimensional ^1H-^1H NOESY spectra of npAβ (*red*) and pS8Aβ (*green*) showing some of the sequential HN-HN NOE peaks. *C*, intensity of HN-HN NOE peaks shown in *B* after calibration with respect to the NOE peak between Gln^{15} side chain protons. Higher intensities of sequential HN-HN peaks for Gly^9–Glu^{11} support a phosphorylation-induced decrease of extended conformation for residues C-terminal to the phosphorylation site. *Error bars* represent S.D. and were estimated on the basis of the signal-to-noise ratio in the spectra.

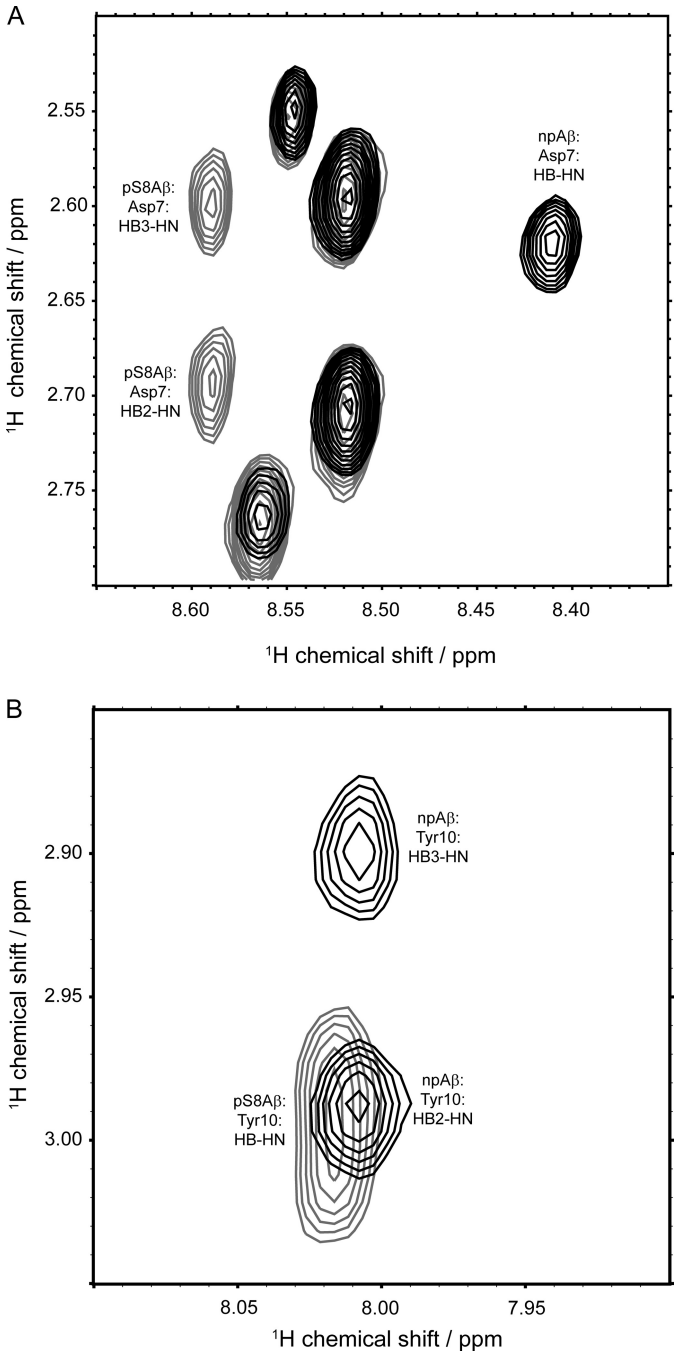

FIGURE 5. **Phosphorylation at Ser^8 differentially influences residues preceding and following the modification site.** *A* and *B*, selected regions of two-dimensional ^{1}H, ^{1}H TOCSY spectra containing the Hβ resonances of Asp^7 (*A*) and Tyr^{10} (*B*). Following phosphorylation at Ser^8, the Hβ resonances of Asp^7 become more dispersed, whereas the Hβ resonances of Tyr^{10} lose a large part of their resolution.

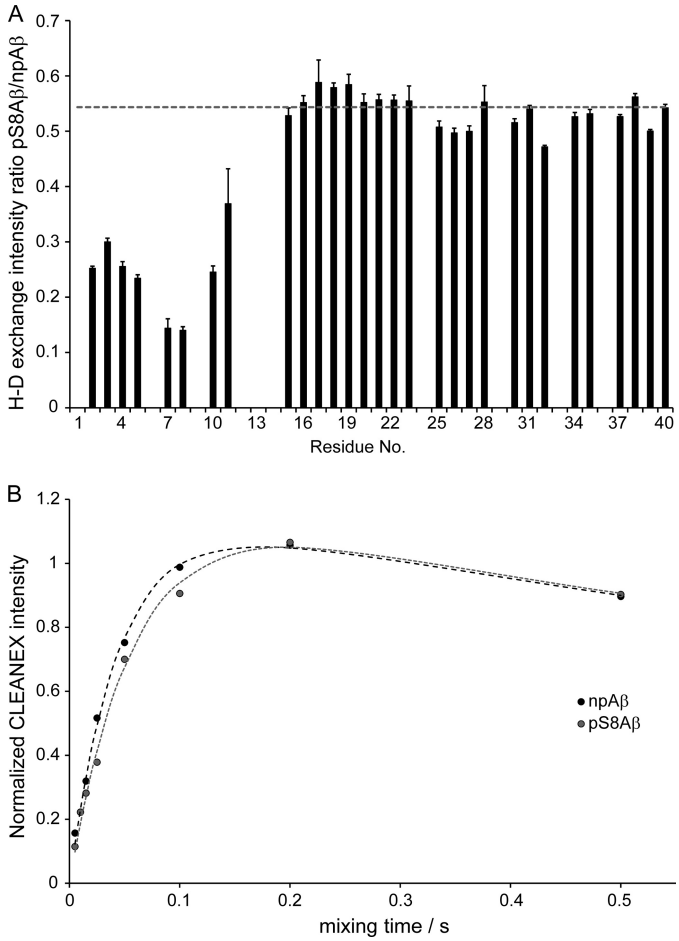

FIGURE 6. **The N-terminal region is more solvent-exposed in insoluble pS8Aβ aggregates than in non-phosphorylated aggregates.** *A*, intensity ratio between the TOCSY cross-peaks of pS8Aβ and npAβ in hydrogen-deuterium (*H-D*) exchange NMR experiments. For residues Gln^{15}–Val^{40}, the observed ratio of ~0.54 (*dashed line*) is due to a lower amount of insoluble aggregates formed by pS8Aβ when compared with npAβ. The prominent drop observed in the intensity ratio of the N-terminal residues indicates a higher solvent exposure of this region in pS8Aβ aggregates. *B*, in one-dimensional CLEANEX NMR experiments, monomeric pS8Aβ shows a smaller collective water-amide proton exchange rate than npAβ, excluding the possibility that the intensity profile of the hydrogen-deuterium exchange NMR data (shown in *A*) arises because of a phosphorylation-induced increase in the intrinsic exchange rates. *Error bars* represent S.D. and were estimated on the basis of the signal-to-noise ratio of the spectra.

insoluble Aβ aggregates were spun down by ultracentrifugation and then resuspended in pure D_2O in a way that unprotected protons could be exchanged with deuterons. Then, after a second run of ultracentrifugation and following dissociation of the pellet with 5% dichloroacetic acid, 95% DMSO, we obtained two-dimensional ^{1}H,^{1}H TOCSY spectra and evaluated the intensity of cross-peaks between backbone amide protons and non-exchangeable aliphatic protons. For residues 15–40, the ratio of cross-peak intensity between pS8Aβ and npAβ was 0.54 ± 0.03 (Fig. 6*A*). Because a similar ratio of ~0.55 was observed for the intensity of non-exchangeable methyl resonances, the lower cross-peak intensity of residues 15–40 is attributed to a lower incorporation of pS8Aβ into insoluble aggregates in agreement with the higher propensity of pS8Aβ to form soluble oligomers (23). However, the intensity ratio dropped even further in the N-terminal residues: the smallest ratio was observed for Asp^7 and Ser^8 at ~0.14 around the phosphorylation site, and the average ratio for flanking residues Ala^2–Arg^5 and Tyr^{10}-Glu^{11} was 0.28 ± 0.05 (Fig. 6*A*).

To investigate whether the lower peak intensity of N-terminal residues in pS8Aβ had its origin in a higher intrinsic exchange rate around the phosphoserine, we evaluated the collective water-amide proton exchange rates of monomeric npAβ and pS8Aβ through a one-dimensional CLEANEX experiments at 15 °C (Fig. 6*B*). Water-amide proton exchange

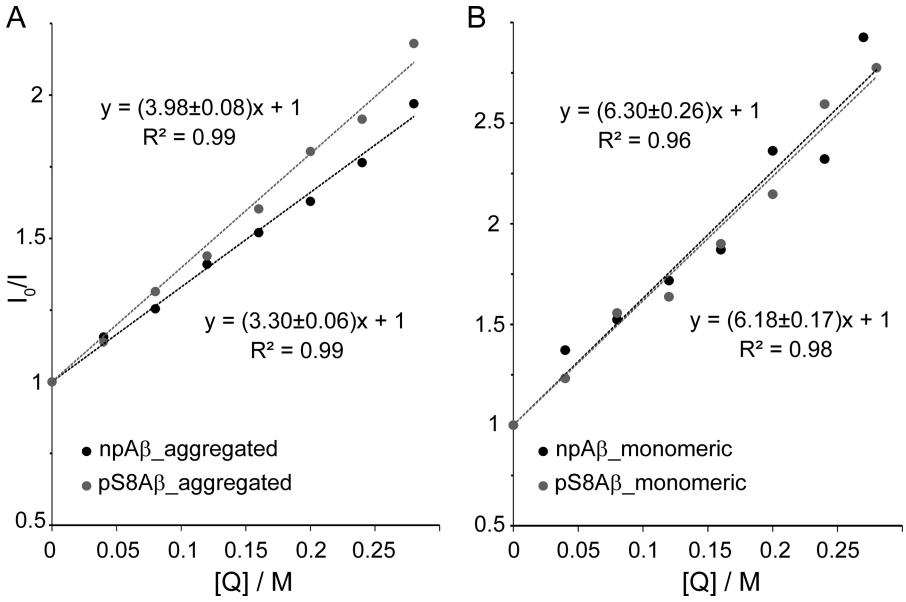

FIGURE 7. **Phosphorylation at Ser[8] increases the solvent exposure of Aβ aggregates, supported by fluorescence dynamic quenching data probing Tyr[10].** The Stern-Volmer relationship between the normalized fluorescence intensity *I* and quencher (acrylamide) concentration *Q* is shown for aggregated (*A*) and monomeric (*B*) Aβ. Although the quenching constants of monomeric npAβ and pS8Aβ are indistinguishable (*B*), aggregated pS8Aβ shows a larger quenching constant.

rate constants of 26.0 ± 2.5 and 20.5 ± 2.9 s^{-1} were obtained for npAβ and pS8Aβ, respectively. Because the intrinsic exchange rate in pS8Aβ is not larger than in npAβ, the possibility that the enhanced efficiency of hydrogen-deuterium exchange in pS8Aβ arises because of its higher intrinsic exchange rate is excluded. Our data thus demonstrate that the peptide backbone in the N-terminal region is more solvent-exposed in insoluble pS8Aβ aggregates than in aggregates of npAβ.

To further investigate the solvent exposure of the N-terminal region of Aβ aggregates, we performed dynamic quenching measurements in which the fluorescence emission of Tyr^{10} was probed in the presence of the neutral quencher acrylamide. When the lifetime of fluorescence excited states does not significantly vary, the quenching constant (the Stern-Volmer constant (K_{SV})), which is obtained through the dependence of fluorescence intensities on quencher concentration, reflects how much the fluorophore is exposed to solvent. For monomeric npAβ and pS8Aβ, similar quenching constants of 6.30 ± 0.26 and 6.18 ± 0.17 M^{-1} were obtained. In contrast, K_{SV} was significantly higher in pS8Aβ (3.98 ± 0.08 M^{-1}) than in npAβ aggregates (3.30 ± 0.06 M^{-1}) (Fig. 7). The higher K_{SV} of pS8Aβ aggregates provides further support for the lower compaction of the N-terminal region of phosphorylated Aβ aggregates.

Phosphorylated Aβ Fibrils Exhibit Distinct Sedimentation Behavior—Phosphorylation at Ser[8] enhances the oligomeric and fibrillar aggregation of Aβ (23). The fibrils generated by npAβ and pS8Aβ are similar in morphology, but they show significant differences in the stability against SDS- and pressure-induced dissociation (24). To further investigate the effects of Ser[8] phosphorylation on the properties of Aβ aggregates, 5-day-aggregated Aβ samples were briefly centrifuged (16,000 × *g* for 30 min), and the pellets and supernatants were examined separately. NMR measurements of the dissociated pellets showed that the concentration of pS8Aβ in the pelleted aggregates was smaller than in the pellet obtained from the npAβ sample (Fig. 8) in agreement with higher CD intensities of pS8Aβ in the supernatant (Fig. 9). EM examination further demonstrated that the pS8Aβ supernatant but not the npAβ supernatant was rich in fibrils (Fig. 10). In addition, the fibrils observed in the supernatant of pS8Aβ exhibited detailed features on their surface that were not present in the few fibrils that were found in the npAβ supernatant (Fig. 10). The data suggest that Ser[8] phosphorylation alters the surface properties of Aβ fibrils in a manner that reduces their higher order assembly and increases the number of dispersed Aβ fibrils.

Discussion

Aβ aggregation proceeds through several steps in which Aβ forms different conformational and assembly states. Although a U-shaped strand-turn-strand conformation of Aβ is a structural motif commonly preserved along the aggregation pathway (27, 28), a high level of conformational rearrangement underlying the interconversion of Aβ aggregates is essential for progression of Aβ aggregation (29). One striking example of the role of conformational plasticity in Aβ aggregation is observed in the turn region around Ser[26] where rigidification of this region by Ser[26] phosphorylation is connected to the prevention of fibrillar Aβ aggregates (26). Similarly, maturation of Aβ fibrillar aggregates in later stages of aggregation involves extension of the β-sheet structure toward the N terminus (30). Moreover, the N-terminal region of Aβ fibrils manifests significant structural polymorphism with various degrees of solvent protection due to variations in experimental conditions (31). Our data demonstrate that the conformational dynamics of Ser[8] and its adjacent residues are significantly affected by phosphorylation. In agreement with the crucial importance of local flexibility for structural remodeling of Aβ aggregates, our hydrogen-

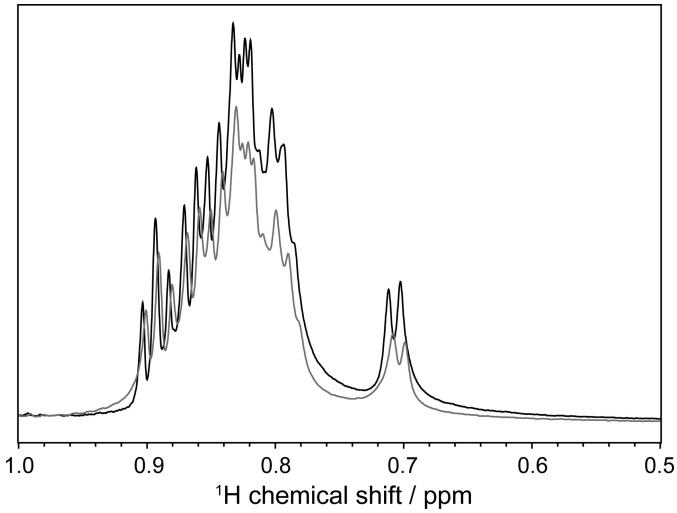

FIGURE 8. **A smaller amount of pS8Aβ than npAβ is incorporated into insoluble Aβ aggregates as indicated by one-dimensional proton NMR spectra of npAβ (*black*) and pS8Aβ (*gray*).** After 5 days of aggregation, the Aβ samples were centrifuged (16,000 × *g* for 30 min), and the pellets were dissociated into monomers by 5% dichloroacetic acid, 95% DMSO and examined by NMR. The signal intensity ratio in the methyl region (between 1 and 0.5 ppm) was ~0.8 for pS8Aβ:npAβ.

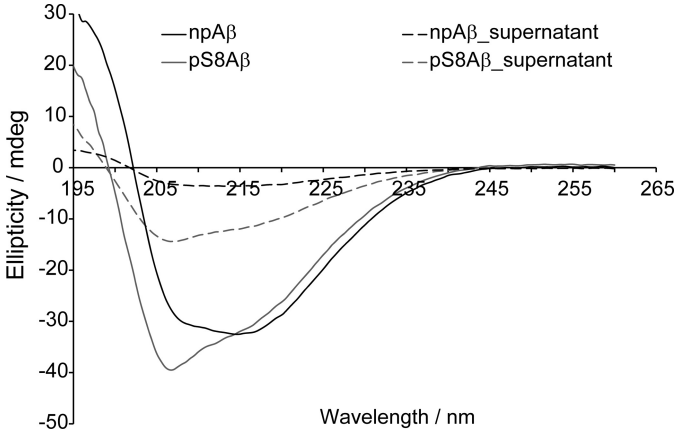

FIGURE 9. **The aggregated pS8Aβ contains higher amounts of soluble Aβ assemblies than npAβ.** After 5 days of aggregation, CD spectra of the whole aggregated samples (*solid lines*) and supernatant fractions (*dotted lines*; 16,000 × *g* for 30 min) were recorded. Stronger CD intensities were observed in the supernatant of aggregated pS8Aβ than in that of npAβ. *mdeg*, millidegrees.

deuterium exchange and fluorescence data demonstrate that Aβ phosphorylation at Ser^8 influences the structure of the N-terminal region of Aβ aggregates, leading to a lower degree of compaction in pS8Aβ aggregates.

Phosphorylation at Ser^8 promotes oligomerization and fibrillation of Aβ (23). In addition, Ser^8 phosphorylation enhances the stability of Aβ aggregates against high pressure- and SDS-induced monomer dissociation (24). Because of a higher compressibility of pS8Aβ aggregates without monomer release, pS8Aβ aggregates undergo a smaller volume decrease upon pressure-assisted monomer dissociation (24). The data reported in the current study demonstrate that phosphorylation at Ser^8 not only influences the stability but also the structure of Aβ aggregates. Although an increase in the stability of pS8Aβ aggregates against pressure-induced dissociation, despite the higher solvent accessibility of pS8Aβ aggregates,

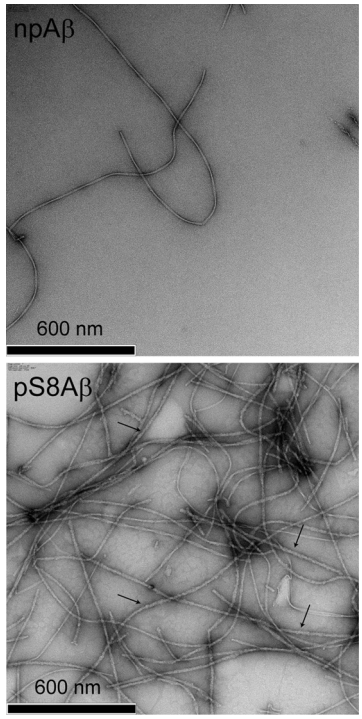

FIGURE 10. **pS8Aβ fibrils exhibit distinct surface properties.** After 5 days of aggregation, EM examination of supernatant fractions (16,000 × *g* for 30 min) revealed many more Aβ fibrils in the pS8Aβ sample than in the npAβ sample in which several pS8Aβ fibrils showed detailed features on their outer surface (examples are indicated by *arrows*).

seems at first sight counterintuitive, it should be noted that the pressure stability and solvent accessibility methods monitor two different aspects of Aβ aggregate structure. For example, in the npAβ aggregates, the N-terminal region of Aβ is rather protected from the solvent as evidenced by hydrogen-deuterium exchange and fluorescence quenching data (Figs. 6 and 7). At the same time, this does not exclude the presence of water-excluded cavities in this region in the structure of npAβ aggregates, and the lower pressure stability of npAβ aggregates (24) suggests that indeed this might be the case. In line with this model, the solvent-exposed N-terminal region of pS8Aβ aggregates would contain fewer water-excluded cavities, resulting in a higher resistance of pS8Aβ aggregates against pressure-induced monomer dissociation. In addition, we showed that the volume change upon monomer release from pS8Aβ aggregates is around 3 times smaller than that of npAβ aggregates (8 *versus* 25 ml/mol), suggesting that the pS8Aβ aggregates have higher compressibility without undergoing monomer release. According to molecular dynamics simulations (24), the increased number of intramolecular electrostatic interactions in pS8Aβ aggregates and their susceptibility to pressure-induced disruption contribute to the higher compressibility of pS8Aβ aggregates without Aβ monomer release. The combined data show that phosphorylation at Ser^8 modulates both the stability and structure of Aβ aggregates.

Despite the largely disordered structure of Aβ in aqueous solution, several short segments of the Aβ sequence exhibit non-random conformational preferences (32). Of special interest in this study is the segment Ser^8–Val^{12}, which adopts a transient turnlike structure (32, 33) and thereby partially brings the

N-terminal region of Aβ close to the functionally important central hydrophobic cluster of Aβ (residues Leu^{17}–Phe^{20}) (34, 35). In addition, residues Phe^{20}–Val^{24} tend to form a helical turn (32), which is in line with the helical propensity of this segment observed in SDS micelle environments and non-aqueous helix-inducing solvents (36–38). Helical propensity of residues His^{13}–Asp^{23} has been suggested to be crucial for the early aggregation of Aβ and its interaction with membranes (39). Local perturbation of Aβ conformation by Ser^8 phosphorylation, as demonstrated by our data, can therefore be associated with subtle long range conformational alterations, further influencing its aggregation behavior. The observation that the fine modulation of Aβ conformation by Ser^8 phosphorylation influences its aggregation is of potential wider interest, especially because Aβ aggregation *in vivo* usually occurs in various environments such as cellular membrane interfaces where interaction with membrane lipids influences Aβ conformation (40, 41).

The N-terminal region of Aβ is host for a wide range of events such as phosphorylation (23), metal binding (28, 42), tyrosine nitration (43), and truncation (19, 20). These events may modulate the role of Aβ in oxidative damage (44) and induction of inflammation (45) and alter the efficiency of prion-like self-propagation (24) and their interaction with biological targets such as cellular lipid membranes (46). Based on the observation that phosphorylation of Ser^8 increases the N-terminal exposure of Aβ aggregates, we hypothesize that phosphorylation might contribute to a mechanism of cross-talk between different N-terminal modifications of Aβ aggregates and thus influence the biochemical maturation of Aβ aggregates (14) and progressive course of AD. This hypothesis remains to be tested by additional experiments probing different N-terminal modifications dependent on Ser^8 phosphorylation.

In conclusion, phosphorylation of Aβ at Ser^8 changes the structure of the N-terminal region of Aβ aggregates in favor of more solvent-exposed conformations. Our data provide experimental support at the molecular level for the potential role of posttranslational modifications in structural polymorphism of amyloids.

Experimental Procedures

Materials—Synthetic npAβ and pS8Aβ were obtained from Peptide Specialty Laboratory (Germany); both had a purity of more than 95% and were used without further purification. The ^{15}N,^{13}C-labeled Aβ1–40 (non-phosphorylated) was purchased from AlexoTech (Sweden); it had a purity above 95% and was used without further purification. For monomerization, the Aβ powders were dissolved in 20 mM NaOH at 2 mg/ml peptide concentration, and after 1 min of sonication and 30 min of shaking in the cold room (4 °C), they were split into 50-μl aliquots, flash frozen in liquid nitrogen, and stored at −80 °C until use.

Transmission Electron Microscopy—For EM examination, aggregated samples of npAβ and pS8Aβ were deposited onto carbon-coated copper mesh grids and negatively stained with 2% (w/v) uranyl acetate. Excess stain was washed away, and the sample grids were allowed to air-dry. Subsequently, the samples were examined using a Philips CM 120 BioTwin transmission electron microscope (Philips Inc., Eindhoven, The Netherlands).

Far-UV CD Spectroscopy—After a two-step solubilization, first in 1,1,1,3,3,3-hexafluoro-2-propanol and then in 100 mM NaOH, synthetic npAβ and pS8Aβ peptide variants were dissolved in 20 mM sodium phosphate (pH adjusted to 7.40) at a concentration of 0.3 mg/ml. CD spectra were recorded on a Chirascan spectropolarimeter using a cuvette with 1-mm path length at 10 °C. The CD spectra were recorded from 260 to 190 nm at 0.5-nm intervals with an acquisition time per data point of 8 s. Temperature control with an accuracy of ±0.5 °C was achieved with a heating/cooling accessory using a Peltier element.

Dynamic Fluorescence Quenching Experiment—Tyr^{10} fluorescence emission spectra of monomeric and aggregated npAβ and pS8Aβ samples (50 μM in 50 mM sodium phosphate, 50 mM NaCl, pH 7.4) were measured in the presence of specified concentrations of the neutral quencher acrylamide. The aggregated Aβ samples were incubated in aggregation-prone conditions (37 °C with gentle stirring) for 72 h. The excitation wavelength was 279 nm, and emission spectra were recorded between 292 and 350 nm. The maximum emission intensity obtained through interpolation was used for Stern-Volmer analysis. K_{SV} was obtained from the following equation.

$$\frac{I_0}{I} = 1 + K_{SV}[Q] \qquad \text{(Eq. 1)}$$

in which I_0 is the maximal emission intensity obtained in the absence of quencher and $[Q]$ is the molar concentration of the quencher.

Two-dimensional Homonuclear NMR Experiments—NMR samples contained 0.4 mg/ml Aβ in 20 mM sodium phosphate buffer, pH 7.2, and measurements were performed at 5 °C. Chemical shift referencing at this temperature was made with respect to external 4,4-dimethyl-4-silapentane-1-sulfonic acid (0.0 ppm). All NMR spectra were processed and analyzed with NMRPipe (47) and Sparky (50). Two-dimensional ^1H,^1H TOCSY and NOESY spectra were acquired on a Bruker (Germany) Avance 800-MHz spectrometer equipped with a cryogenic probe. The time domain data contained 2,048 and 600 complex data points in t2 and t1, respectively. MLEV17 was used for mixing in the TOCSY experiment with a total duration of 60 ms. The mixing time in the NOESY experiment was 200 ms. Water signals were suppressed through a WATERGATE element. ^1H resonance assignments were made on the basis of the two-dimensional ^1H,^1H TOCSY and NOESY spectra. The combined HN and HA chemical shift perturbation (CSP) induced by Ser^8 phosphorylation was evaluated using the following equation.

$$CSP = \sqrt{(\Delta HN)^2 + (\Delta HA)^2} \qquad \text{(Eq. 2)}$$

Pulsed Field Gradient NMR—Pulsed field gradient NMR experiments were performed on a Bruker AMX 600-MHz spectrometer equipped with a triple resonance cryogenic probe. The sample contained dioxane as an internal hydrodynamic radius standard and viscosity probe. Sixteen one-dimensional ^1H spectra were collected as a function of gradient amplitude using the stimulated echo sequence with bipolar gradient pulses with gradient strengths increasing from 0.674 to 32.030 G/cm (after correction for the sine shape of the gradient pulses) in a linear manner. The gradient distance (Δ) was 200 ms, and the total

gradient length (δ) was 4 ms. Peaks in the aliphatic region of the ^{1}H spectra were picked, and the apparent translational diffusion coefficients were calculated after fitting the intensity *versus* gradient strength data to a corresponding diffusion equation.

Two-dimensional and Three-dimensional Heteronuclear NMR Experiments—NMR samples containing 0.4 mg/ml ^{15}N,^{13}C-labeled Aβ (20 mM sodium phosphate, pH 7.2) were measured at 5 °C on a 700-MHz Bruker spectrometer with cryogenic probe. Chemical shift referencing was made with respect to an internal 4,4-dimethyl-4-silapentane-1-sulfonic acid standard (0.0 ppm). The ^{1}H,^{15}N heteronuclear single quantum correlation, ^{1}H,^{13}C heteronuclear single quantum correlation, HNCA, and HNCO experiments were used for backbone assignment. The residue-specific random coil index and corresponding squared order parameter (S^2) values were calculated through the random coil index web server.

Hydrogen-Deuterium Exchange NMR Experiments—npAβ and pS8Aβ samples (50 μM) in PBS were incubated in aggregation-prone conditions (37 °C with gentle stirring) for 7 days. Subsequently, aggregated Aβ samples were ultracentrifuged (100,000 × g at 25 °C) for 4 h, and the pellet was dried using strips of filter paper, resuspended in D_2O with gentle vortexing, and incubated at room temperature for 1 h to allow for forward exchange from D_2O to exchangeable amide protons. After D_2O treatment, insoluble Aβ aggregates were again collected by ultracentrifugation (100,000 × g at 25 °C for 4 h) and carefully dried to remove residual D_2O. The collected Aβ aggregates were then dissolved in 250 μl of 5% dichloroacetic acid, 95% DMSO mixture and immediately transferred to an NMR tube to start data acquisition on an 800-MHz Bruker NMR spectrometer. One-dimensional ^{1}H, two-dimensional ^{1}H, ^{1}H TOCSY, and NOESY spectra were obtained. Mixing times of 60 ms for TOCSY and 200 and 300 ms for NOESY experiments were used. Peak assignments were made through a standard homonuclear sequential assignment strategy and further checked with the assignments reported previously (48). The relative extent of hydrogen-deuterium exchange in npAβ and pS8Aβ aggregates was evaluated through comparing the TOCSY cross-peak intensities between the two peptides.

Water-Amide Proton Exchange Rates—Intrinsic water-amide proton rates in monomeric npAβ and pS8Aβ samples (75 μM; buffered with 20 mM sodium phosphate, pH 7.4) were measured through one-dimensional CLEANEX-PM experiments on a 700-MHz Bruker spectrometer at 15 °C. In this experiment, a selective water excitation pulse was followed by a mixing time (τ_m) of durations 5, 10, 15, 25, 50, 100, 200, and 500 ms during which chemical exchange between water and amide protons takes place. The global intensity of amide protons as a function of mixing time was fitted to the following equation.

$$\frac{V}{V_0} = \frac{k \cdot [\exp(-R_{1B} \cdot \tau_m) - \exp[-(R_{1A} + k) \cdot \tau_m]]}{(R_{1A} + k - R_{1B})} \quad \text{(Eq. 3)}$$

where V_0 is the intensity in a control experiment, k is the normalized rate constant related to the forward exchange rate constant between water and amide protons, and R_{1A} and R_{1B} are apparent longitudinal relaxation rates for protein and water (49).

Author Contributions—N. R.-G. designed and conducted the NMR, fluorescence, and CD experiments; analyzed the results; and wrote the paper. S. K. contributed to CD experiments. J. W. conceived the project. M. Z. conceived the project and wrote the paper.

Acknowledgments—We thank Dr. Dietmar Riedel and Gudrun Heim for the EM examination of Aβ samples.

References

1. Haass, C., and Selkoe, D. J. (2007) Soluble protein oligomers in neurodegeneration: lessons from the Alzheimer's amyloid β-peptide. *Nat. Rev. Mol. Cell Biol.* **8,** 101–112
2. Schmid, A. W., Fauvet, B., Moniatte, M., and Lashuel, H. A. (2013) α-Synuclein post-translational modifications as potential biomarkers for Parkinson disease and other synucleinopathies. *Mol. Cell. Proteomics* **12,** 3543–3558
3. Russell, C. L., Koncarevic, S., and Ward, M. A. (2014) Post-translational modifications in Alzheimer's disease and the potential for new biomarkers. *J. Alzheimers Dis.* **41,** 345–364
4. Tenreiro, S., Eckermann, K., and Outeiro, T. F. (2014) Protein phosphorylation in neurodegeneration: friend or foe? *Front. Mol. Neurosci.* **7,** 42
5. Kumar, S., Wirths, O., Stüber, K., Wunderlich, P., Koch, P., Theil, S., Rezaei-Ghaleh, N., Zweckstetter, M., Bayer, T. A., Brüstle, O., Thal, D. R., and Walter, J. (2016) Phosphorylation of the amyloid β-peptide at Ser26 stabilizes oligomeric assembly and increases neurotoxicity. *Acta Neuropathol.* **131,** 525–537
6. Rijal Upadhaya, A., Kosterin, I., Kumar, S., von Arnim, C. A., Yamaguchi, H., Fändrich, M., Walter, J., and Thal, D. R. (2014) Biochemical stages of amyloid-β peptide aggregation and accumulation in the human brain and their association with symptomatic and pathologically preclinical Alzheimer's disease. *Brain* **137,** 887–903
7. McFarland, M. A., Ellis, C. E., Markey, S. P., and Nussbaum, R. L. (2008) Proteomics analysis identifies phosphorylation-dependent α-synuclein protein interactions. *Mol. Cell. Proteomics* **7,** 2123–2137
8. Paleologou, K. E., Oueslati, A., Shakked, G., Rospigliosi, C. C., Kim, H. Y., Lamberto, G. R., Fernandez, C. O., Schmid, A., Chegini, F., Gai, W. P., Chiappe, D., Moniatte, M., Schneider, B. L., Aebischer, P., Eliezer, D., Zweckstetter, M., Masliah, E., and Lashuel, H. A. (2010) Phosphorylation at S87 is enhanced in synucleinopathies, inhibits α-synuclein oligomerization, and influences synuclein-membrane interactions. *J. Neurosci.* **30,** 3184–3198
9. Gonçalves, S., and Outeiro, T. F. (2013) Assessing the subcellular dynamics of α-synuclein using photoactivation microscopy. *Mol. Neurobiol.* **47,** 1081–1092
10. Oueslati, A., Schneider, B. L., Aebischer, P., and Lashuel, H. A. (2013) Polo-like kinase 2 regulates selective autophagic α-synuclein clearance and suppresses its toxicity *in vivo*. *Proc. Natl. Acad. Sci. U.S.A.* **110,** E3945–E3954
11. Tenreiro, S., Reimão-Pinto, M. M., Antas, P., Rino, J., Wawrzycka, D., Macedo, D., Rosado-Ramos, R., Amen, T., Waiss, M., Magalhães, F., Gomes, A., Santos, C. N., Kaganovich, D., and Outeiro, T. F. (2014) Phosphorylation modulates clearance of α-synuclein inclusions in a yeast model of Parkinson's disease. *PLoS Genet.* **10,** e1004302
12. Mahul-Mellier, A. L., Fauvet, B., Gysbers, A., Dikiy, I., Oueslati, A., Georgeon, S., Lamontanara, A. J., Bisquertt, A., Eliezer, D., Masliah, E., Halliday, G., Hantschel, O., and Lashuel, H. A. (2014) c-Abl phosphorylates α-synuclein and regulates its degradation: implication for α-synuclein clearance and contribution to the pathogenesis of Parkinson's disease. *Hum. Mol. Genet.* **23,** 2858–2879
13. Kumar, S., Singh, S., Hinze, D., Josten, M., Sahl, H. G., Siepmann, M., and Walter, J. (2012) Phosphorylation of amyloid-β peptide at serine 8 attenuates its clearance via insulin-degrading and angiotensin-converting enzymes. *J. Biol. Chem.* **287,** 8641–8651
14. Thal, D. R., Walter, J., Saido, T. C., and Fändrich, M. (2015) Neuropathology and biochemistry of Aβ and its aggregates in Alzheimer's disease. *Acta Neuropathol.* **129,** 167–182

15. Fändrich, M., Schmidt, M., and Grigorieff, N. (2011) Recent progress in understanding Alzheimer's β-amyloid structures. *Trends Biochem. Sci.* **36,** 338–345
16. Tycko, R., and Wickner, R. B. (2013) Molecular structures of amyloid and prion fibrils: consensus versus controversy. *Acc. Chem. Res.* **46,** 1487–1496
17. Di Fede, G., Catania, M., Morbin, M., Rossi, G., Suardi, S., Mazzoleni, G., Merlin, M., Giovagnoli, A. R., Prioni, S., Erbetta, A., Falcone, C., Gobbi, M., Colombo, L., Bastone, A., Beeg, M., Manzoni, C., Francescucci, B., Spagnoli, A., Cantù, L., Del Favero, E., Levy, E., Salmona, M., and Tagliavini, F. (2009) A recessive mutation in the APP gene with dominant-negative effect on amyloidogenesis. *Science* **323,** 1473–1477
18. Ono, K., Condron, M. M., and Teplow, D. B. (2010) Effects of the English (H6R) and Tottori (D7N) familial Alzheimer disease mutations on amyloid β-protein assembly and toxicity. *J. Biol. Chem.* **285,** 23186–23197
19. Schilling, S., Zeitschel, U., Hoffmann, T., Heiser, U., Francke, M., Kehlen, A., Holzer, M., Hutter-Paier, B., Prokesch, M., Windisch, M., Jagla, W., Schlenzig, D., Lindner, C., Rudolph, T., Reuter, G., Cynis, H., Montag, D., Demuth, H. U., and Rossner, S. (2008) Glutaminyl cyclase inhibition attenuates pyroglutamate Aβ and Alzheimer's disease-like pathology. *Nat. Med.* **14,** 1106–1111
20. Bouter, Y., Dietrich, K., Wittnam, J. L., Rezaei-Ghaleh, N., Pillot, T., Papot-Couturier, S., Lefebvre, T., Sprenger, F., Wirths, O., Zweckstetter, M., and Bayer, T. A. (2013) N-truncated amyloid β (Aβ) 4–42 forms stable aggregates and induces acute and long-lasting behavioral deficits. *Acta Neuropathol.* **126,** 189–205
21. Gardberg, A. S., Dice, L. T., Ou, S., Rich, R. L., Helmbrecht, E., Ko, J., Wetzel, R., Myszka, D. G., Patterson, P. H., and Dealwis, C. (2007) Molecular basis for passive immunotherapy of Alzheimer's disease. *Proc. Natl. Acad. Sci. U.S.A.* **104,** 15659–15664
22. Haupt, C., Leppert, J., Rönicke, R., Meinhardt, J., Yadav, J. K., Ramachandran, R., Ohlenschläger, O., Reymann, K. G., Görlach, M., and Fändrich, M. (2012) Structural basis of β-amyloid-dependent synaptic dysfunctions. *Angew. Chem. Int. Ed. Engl.* **51,** 1576–1579
23. Kumar, S., Rezaei-Ghaleh, N., Terwel, D., Thal, D. R., Richard, M., Hoch, M., Mc Donald, J. M., Wüllner, U., Glebov, K., Heneka, M. T., Walsh, D. M., Zweckstetter, M., and Walter, J. (2011) Extracellular phosphorylation of the amyloid β-peptide promotes formation of toxic aggregates during the pathogenesis of Alzheimer's disease. *EMBO J.* **30,** 2255–2265
24. Rezaei-Ghaleh, N., Amininasab, M., Kumar, S., Walter, J., and Zweckstetter, M. (2016) Phosphorylation modifies the molecular stability of β-amyloid deposits. *Nat. Commun.* **7,** 11359
25. Berjanskii, M. V., and Wishart, D. S. (2005) A simple method to predict protein flexibility using secondary chemical shifts. *J. Am. Chem. Soc.* **127,** 14970–14971
26. Rezaei-Ghaleh, N., Amininasab, M., Giller, K., Kumar, S., Stündl, A., Schneider, A., Becker, S., Walter, J., and Zweckstetter, M. (2014) Turn plasticity distinguishes different modes of amyloid-β aggregation. *J. Am. Chem. Soc.* **136,** 4913–4919
27. Abelein, A., Abrahams, J. P., Danielsson, J., Gräslund, A., Jarvet, J., Luo, J., Tiiman, A., and Wärmländer, S. K. (2014) The hairpin conformation of the amyloid β peptide is an important structural motif along the aggregation pathway. *J. Biol. Inorg. Chem.* **19,** 623–634
28. Rezaei-Ghaleh, N., Giller, K., Becker, S., and Zweckstetter, M. (2011) Effect of zinc binding on β-amyloid structure and dynamics: implications for Aβ aggregation. *Biophys. J.* **101,** 1202–1211
29. Hoyer, W., and Härd, T. (2008) Interaction of Alzheimer's Aβ peptide with an engineered binding protein—thermodynamics and kinetics of coupled folding-binding. *J. Mol. Biol.* **378,** 398–411
30. Scheidt, H. A., Morgado, I., Rothemund, S., Huster, D., and Fändrich, M. (2011) Solid-state NMR spectroscopic investigation of Aβ protofibrils: implication of a β-sheet remodeling upon maturation into terminal amyloid fibrils. *Angew. Chem. Int. Ed. Engl.* **50,** 2837–2840
31. Kodali, R., Williams, A. D., Chemuru, S., and Wetzel, R. (2010) Aβ(1–40) forms five distinct amyloid structures whose β-sheet contents and fibril stabilities are correlated. *J. Mol. Biol.* **401,** 503–517
32. Riek, R., Güntert, P., Döbeli, H., Wipf, B., and Wüthrich, K. (2001) NMR studies in aqueous solution fail to identify significant conformational differences between the monomeric forms of two Alzheimer peptides with widely different plaque-competence, Aβ(1–40)(ox) and Aβ(1–42)(ox). *Eur. J. Biochem.* **268,** 5930–5936
33. Lim, K. H., Henderson, G. L., Jha, A., and Louhivuori, M. (2007) Structural, dynamic properties of key residues in Aβ amyloidogenesis: implications of an important role of nanosecond timescale dynamics. *Chembiochem* **8,** 1251–1254
34. Hilbich, C., Kisters-Woike, B., Reed, J., Masters, C. L., and Beyreuther, K. (1992) Substitutions of hydrophobic amino acids reduce the amyloidogenicity of Alzheimer's disease βA4 peptides. *J. Mol. Biol.* **228,** 460–473
35. Das, A. K., Rawat, A., Bhowmik, D., Pandit, R., Huster, D., and Maiti, S. (2015) An early folding contact between Phe19 and Leu34 is critical for amyloid-β oligomer toxicity. *ACS Chem. Neurosci.* **6,** 1290–1295
36. Coles, M., Bicknell, W., Watson, A. A., Fairlie, D. P., and Craik, D. J. (1998) Solution structure of amyloid β-peptide(1–40) in a water-micelle environment. Is the membrane-spanning domain where we think it is? *Biochemistry* **37,** 11064–11077
37. Shao, H., Jao, S., Ma, K., and Zagorski, M. G. (1999) Solution structures of micelle-bound amyloid β-(1–40) and β-(1–42) peptides of Alzheimer's disease. *J. Mol. Biol.* **285,** 755–773
38. Jarvet, J., Danielsson, J., Damberg, P., Oleszczuk, M., and Gräslund, A. (2007) Positioning of the Alzheimer Aβ(1–40) peptide in SDS micelles using NMR and paramagnetic probes. *J. Biomol. NMR* **39,** 63–72
39. Vivekanandan, S., Brender, J. R., Lee, S. Y., and Ramamoorthy, A. (2011) A partially folded structure of amyloid-β(1–40) in an aqueous environment. *Biochem. Biophys. Res. Commun.* **411,** 312–316
40. Morgado, I., and Garvey, M. (2015) Lipids in amyloid-β processing, aggregation, and toxicity. *Adv. Exp. Med. Biol.* **855,** 67–94
41. Qiang, W., Akinlolu, R. D., Nam, M., and Shu, N. (2014) Structural evolution and membrane interaction of the 40-residue β amyloid peptides: differences in the initial proximity between peptides and the membrane bilayer studied by solid-state nuclear magnetic resonance spectroscopy. *Biochemistry* **53,** 7503–7514
42. Faller, P., and Hureau, C. (2009) Bioinorganic chemistry of copper and zinc ions coordinated to amyloid-β peptide. *Dalton Trans.* 1080–1094
43. Kummer, M. P., Hermes, M., Delekarte, A., Hammerschmidt, T., Kumar, S., Terwel, D., Walter, J., Pape, H. C., König, S., Roeber, S., Jessen, F., Klockgether, T., Korte, M., and Heneka, M. T. (2011) Nitration of tyrosine 10 critically enhances amyloid β aggregation and plaque formation. *Neuron* **71,** 833–844
44. Parthasarathy, S., Long, F., Miller, Y., Xiao, Y., McElheny, D., Thurber, K., Ma, B., Nussinov, R., and Ishii, Y. (2011) Molecular-level examination of Cu^{2+} binding structure for amyloid fibrils of 40-residue Alzheimer's β by solid-state NMR spectroscopy. *J. Am. Chem. Soc.* **133,** 3390–3400
45. Cameron, B., and Landreth, G. E. (2010) Inflammation, microglia, and Alzheimer's disease. *Neurobiol. Dis.* **37,** 503–509
46. Williamson, M. P., Suzuki, Y., Bourne, N. T., and Asakura, T. (2006) Binding of amyloid β-peptide to ganglioside micelles is dependent on histidine-13. *Biochem. J.* **397,** 483–490
47. Delaglio, F., Grzesiek, S., Vuister, G. W., Zhu, G., Pfeifer, J., and Bax, A. (1995) NMRPipe: a multidimensional spectral processing system based on UNIX pipes. *J. Biomol. NMR* **6,** 277–293
48. Whittemore, N. A., Mishra, R., Kheterpal, I., Williams, A. D., Wetzel, R., and Serpersu, E. H. (2005) Hydrogen-deuterium (H/D) exchange mapping of Aβ1–40 amyloid fibril secondary structure using nuclear magnetic resonance spectroscopy. *Biochemistry* **44,** 4434–4441
49. Hwang, T. L., van Zijl, P. C., and Mori, S. (1998) Accurate quantitation of water-amide proton exchange rates using the phase-modulated CLEAN chemical EXchange (CLEANEX-PM) approach with a Fast-HSQC (FHSQC) detection scheme. *J. Biomol. NMR* **11,** 221–226
50. Goddard, T. D., and Kneller, D. G. (2007) *Sparky 3*, University of California, San Francisco, CA

Phosphorylation Interferes with Maturation of Amyloid-β Fibrillar Structure in the N Terminus

Nasrollah Rezaei-Ghaleh, Sathish Kumar, Jochen Walter and Markus Zweckstetter

J. Biol. Chem. 2016, 291:16059-16067.
doi: 10.1074/jbc.M116.728956 originally published online June 1, 2016